Membrane and Water Treatment, *Vol. 16, No. 4 (2025) 165-176*
https://doi.org/10.12989/mwt.2025.16.4.165

Modification of porous waste-sugarcane-bagasse-based carbon aerogel electrode for MCDI desalination

Ngan Tuan Nguyen[1,2,3], Van Vien Nguyen[1,2], Thanh Tung Nguyen[3], My Linh Nguyen[4], Hoang Long Ngo[*3] and Thai Hoang Nguyen[**1,2]

[1]*Faculty of Chemistry, University of Science – Ho Chi Minh City, Ho Chi Minh City 700000, Vietnam*
[2]*Vietnam National University Ho Chi Minh City (VNUHCM), Ho Chi Minh City 700000, Vietnam*
[3]*NTT Hi-Tech Institute, Nguyen Tat Thanh University, Ho Chi Minh City 700000, Vietnam*
[4]*Department of Environmental Engineering Technology, Faculty for High Quality Training, HCMC University of Technology and Education, Ho Chi Minh City 700000, Vietnam*

(Received November 19, 2024, Revised February 17, 2025, Accepted February 28, 2025)

Abstract. The utilization of waste sugarcane bagasse in order to reduce landfill residue and CO_2 emission is very crucial. In this research, we present a low-cost and easily accessible approach to fabricating cellulose aerogel from waste sugarcane bagasse using a NaOH/Urea/H_2O gelation solution with different amounts of urea as cross-linking agent. The resulting cellulose aerogels were carbonized and activated to produce activated cellulose carbon aerogel (SB-ACCA). Among the samples, the material with a cellulose:urea ratio of 1:1, designated as SB-ACCA-1.0, exhibited outstanding properties, including the highest BET surface area of 642.3 m^2 g^{-1} together with a high specific capacitance of 96.5 F g^{-1}. These properties both contribute to its significant salt adsorption capacity of 19.49 mg g^{-1} at 1.2 V, which could be further enhanced to 23.91 mg g^{-1} at 1.4 V. These results reveal a viable pathway for utilizing waste sugarcane bagasse and numerous types of agricultural wastes to develop cellulose carbon aerogel electrodes for capacitive deionization in the desalination of salt water, as well as other advanced materials for different environmental applications.

Keywords: activated cellulose carbon aerogel; desalination; membrane capacitive deionization; urea; waste sugarcane bagasse

1. Introduction

One of Vietnam's most significant industrial crops is sugarcane, with the plantation area covering around 127,000 hectares. In the 2020 – 2021 season, around 0.763 million tons of sugar was produced from about 7.498 million tons of sugarcane (Nguyen *et al*. 2022b). However, after industrial processing of sugarcane, including the cleaning and the juice extraction, the sugarcane bagasse byproduct is discarded as residue in large quantity (Anukam *et al*. 2016). About 270 tons of bagasse is disposed for every 1,000 tons of sugarcane (Wuri *et al*. 2021). However, very little amount of waste sugarcane bagasse could be utilized, mostly as biosorbent for organic dyes and heavy metals (Lemessa *et al*. 2023, Ong *et al*. 2010, Safa *et al*. 2018). As a result, sugarcane bagasse is burned as a solid waste disposal method, which may lead to many environmental issues. Therefore, it is absolutely crucial that the waste sugarcane bagasse be handled appropriately, or be converted into something more valuable (Alokika *et al*. 2021).

Since sugarcane bagasse contains a large amount of cellulose (32 – 45%), hemicellulose (20 – 32%), lignin (17 – 32%), ashes (1 – 9%) and other component (2%) (Arni 2018, Karp *et al*. 2013, Yao *et al*. 2015), it is an economical raw materials for a variety of industries, such as paper making, biofuel, biogas, biochar and bioenergy (Ajala *et al*. 2021, Bhatnagar *et al*. 2015, Hiranobe *et al*. 2024). Its high cellulose content makes it one of the most cost-effective and sustainable sources of cellulose (Sun *et al*. 2004a, Thiangtham *et al*. 2019, Wulandari *et al*. 2016). This cellulose can be transformed into various types of new materials, such as cellulose acetate membrane (El-Gendi *et al*. 2012, Katariya and Pate 2022) for membrane water desalination and nanofiltration, or employed as hydrophilic modifier for other types of membrane (Yang *et al*. 2019).

Recently, there have been some researches on the use of sugarcane bagasse as a base material for the synthesis of aerogel (Kumar *et al*. 2021), including pristine cellulose aerogel (CA) or pyrolyzed cellulose carbon aerogel (CCA), which can be used in various applications of thermal insulation (Thai *et al*. 2020), oil absorption (Li *et al*. 2021a, Li *et al*. 2021b, Thai *et al*. 2020), and water pollution treatment (Ahamad *et al*. 2019, Lei *et al*. 2021, Sun *et al*. 2021). Thanks to their adjustable pore structure, wide density variation, good electrical conductivity, high mesoporous volume and large surface area, as well as their low cost and ready availability, cellulose carbon aerogel derived from biomass and biowaste has become one of the up-and-coming electrode materials for the desalination of brackish or seawater via membrane capacitive deionization (MCDI)

[*]Corresponding author, Ph.D.,
E-mail: longnh@ntt.edu.vn

[**]Co-corresponding author, Ph.D., Associate Professor,
E-mail: nthoang@hcmus.edu.vn

ISSN: 2005-8624 (Print), 2092-7037 (Online)

Table 1 A performance comparison between Zr-BADS and other fillers

Carbon aerogel samples	Cellulose: Urea ratio
SB-ACCA-0.75	1:0.75
SB-ACCA-1.0	1:1.0
SB-ACCA-1.5	1:1.5

technology (Nguyen *et al*. 2022a, 2023a, b, 2024, Tran *et al*. 2022). Moreover, their adsorption properties can be further enhanced by tailoring their structures, which can be achieved through modifying the amount of cross-linking agent in the structure of the carbon aerogel (Nguyen *et al*. 2023b), or employing different types of cross-linking agents (Nguyen *et al*. 2024). The MCDI was employed as it was proven to be superior compared the CDI process in terms of salt removal efficiency and prevention of the "co-ion" effect (Kim and Rhim 2016).

In this research, waste sugarcane bagasse was converted into MCDI-utilized cellulose carbon aerogel electrodes using different urea content. The composition of the fabricated carbon aerogel, together with their physicochemical and electrochemical properties, were intensively characterized. Their desalination performance was evaluated through the NaCl adsorption capability using batch mode MCDI.

2. Experimental

2.1 Materials and chemicals

Sugarcane bagasses were collected from local markets near Thu Duc City, Ho Chi Minh City, Vietnam. Graphite sheet (200 µm in thickness) was acquired from Mineral Seal (USA). Polyvinyl alcohol (PVA) and glutaric anhydride (GA) were purchased from Acros, Belgium. Commercial anion-exchange membrane (AEM, 100 µm in thickness) was supplied from Liaoning Yichen Membrane Technology. Sodium hydroxide, formic acid, acetic acid, hydrogen peroxide, urea, potassium hydroxide, and sodium chloride were obtained from Sigma Aldrich (USA). All reagents were used as received without any further purification.

2.2 Fabrication of activated cellulose carbon aerogel from sugarcane bagasse

Cellulose was purified from the biomass using the purification process of cellulose from corn stalks based on previous publications of our research group (Nguyen *et al*. 2022a). Briefly, the collected sugarcane bagasses were boiled at 100 ºC to remove the carbohydrates, pulverized into fine powder, then the powder was treated with 4% NaOH solution and the mixture of H_2O_2: HCOOH: CH_3COOH to remove the lignin and hemicellulose. After each step, the powder was filtered, washed with distilled water until neutral pH, and dried for 12 h at 70 ºC to acquire sugarcane-bagasse-derived cellulose (SB-Cellulose).

SB-Cellulose was then mixed with the mixture of NaOH: Urea: H_2O (with different cellulose: urea ratio) for 4 h at -5 ºC. The obtained solid was dried at 50 ºC for 12 h, followed by the solvent exchange in distilled water until neutral pH. The as-prepared suspension was frozen in a freezer for 24 h at -80 ºC and then freeze-dried for 48 h at -80 ºC and 1 MPa to yield the sugarcane-bagasse-based cellulose aerogel (SB-CA-x).

SB-CA-x was carbonized in N_2 atmosphere for 2 h at 800 ºC to obtain sugarcane bagasse cellulose carbon aerogel (SB-CCA-x), which was then activated by immersing in a 3 M KOH solution for 12 h at room temperature and subsequently calcining for 2 h at 700 ºC to obtain sugarcane-bagasse-derived activated cellulose carbon aerogel (SB-ACCA-x) samples, which were denoted as presented in Table 1.

2.3 Preparation of activated cellulose carbon aerogel electrodes

The preparation of SB-ACCA electrodes was conducted using the curing agents consisting of 6% aqueous polyvinyl alcohol (PVA) and glutaric anhydride (GA) (Ngo *et al*. 2022). First, the mixture of 6% PVA solution and GA was stirred for 1 h, then SB-ACCA powders (with SB-ACCA: PVA/GA ratio of 1: 9) were added, and the mixture was homogenized for 10 minutes at 15,000 rpm. The resulting slurry was coated onto a graphite sheet (200 mm x 300 mm x 200 µm) by the doctor blade techniques. Last, SB-ACCA electrodes were dried for 4 h at 120 °C.

2.4 Physicochemical and electrochemical characterizations

The mass and the dimensions of the cellulose aerogel sample was measured by an analytical balance (Precisa XR 125SM) and a digital caliper (Titan), respectively. The density (ρ) and porosity (P) are calculated using Eqs. 1 and 2 (Anovitz and Cole 2015, Wang *et al*. 2012a):

$$\rho = \frac{m}{V} \quad (1)$$

$$P = 1 - \frac{\rho}{\rho_c} \quad (2)$$

with m being the sample mass (g) and V being the sample volume (cm^3), ρ being the sample density (g cm^{-3}) and ρ_c = 1.528 g cm^{-3} being the bulk density of cellulose from literature (Shi *et al*. 2019).

Fourier Transform Infrared (FT-IR) spectra were acquired recorded using a Cary 630 FTIR (Agilent Tech. Inc., CA). X-ray diffraction (XRD) patterns were obtained from 10º to 70º using a D8 ADVANCE X-ray Diffractometer (Bruker AXS) with CuK_α radiation (λ = 0.154 nm). Scanning Electron Microscope (SEM) analysis was performed using JSM-IT500 Microscope (JEOL). Nitrogen adsorption-desorption isotherms were measured using *Micromeritics* Gemini *VII* (USA), and the surface areas were determined using Brunauer–Emmer–Teller (BET) method. Raman spectra was recorded using an XploRa Plus Raman microscope system (Horiba, Japan).

Cyclic voltammetry (CV) analysis was carried out using an Autolab PGSTAT 302 N (Eco-chemie) in a standard

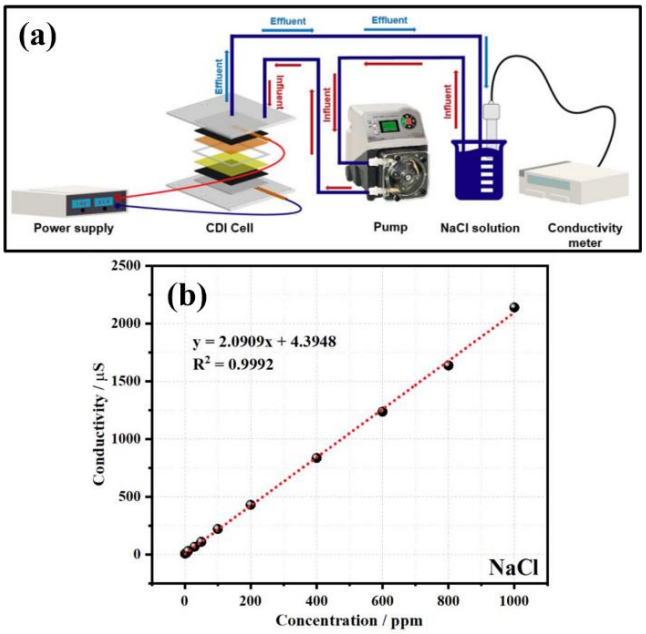

Fig. 1 MCDI system (a) and calibration curve for ionic conductivity vs. NaCl concentration (b)

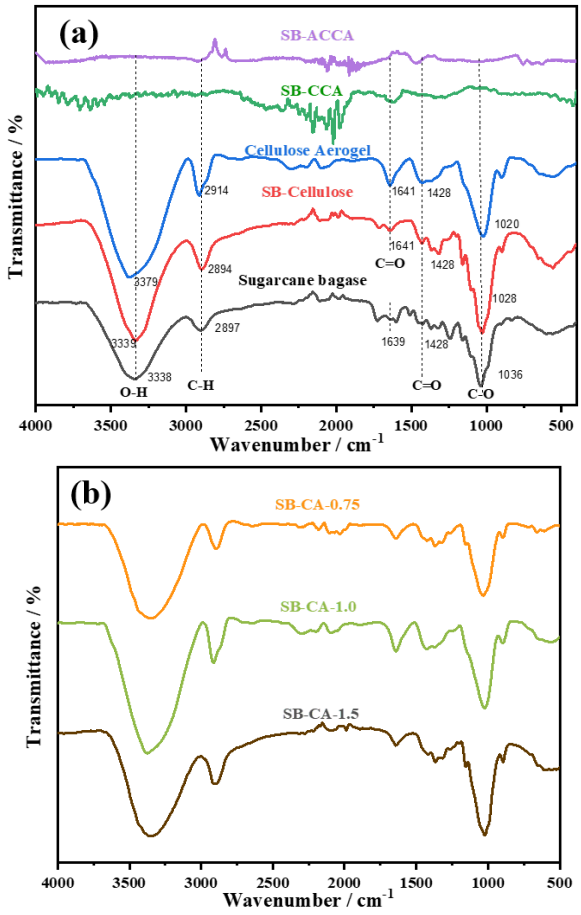

Fig. 2. FT-IR spectra of (a) different waste-sugarcane-bagasse-derived materials and (b) SB-CA-x materials

three-electrode electrochemical cell, with the fabricated carbon aerogel electrode (3.0 x 2.5 cm) being the working electrode, Pt being the counter electrode, and Ag/AgCl being the reference electrode, in aqueous 0.5 M NaCl electrolyte. Specific capacitance values of the carbon aerogel electrodes were calculated from Eq. 3.

$$C_s = \frac{1}{2\times m\times v\times \Delta E} \times \int IdE \quad (3)$$

with C_s being the specific capacitance (F g^{-1}), $\int IdE$ being the integrated area of the CV curve, m being the electrode mass (g), v being the potential scan rate (V s^{-1}), and ΔE being the potential window width (V).

Galvanostatic charge-discharge (GCD) measurements were conducted in 0.5 M NaCl electrolyte using a Lanhe CT3001A Battery testing system with two fabricated carbon aerogel electrodes (1.0 x 1.0 cm). Specific capacitance values of the carbon aerogel electrodes from the GCD plots were calculated from Eq. 4.

$$C_s = \frac{I\ x\ t}{m\ x\ V} \quad (4)$$

with C_s being the specific capacitance (F g^{-1}), I being the applied potential (A), t being the charge – discharge time (s), m being the electrode mass (g), and V being the potential window width (V).

2.5 Desalination capability

The desalination capability was measured on the MCDI system as presented in Fig. 1 (Ngo *et al*. 2022), with the CDI cell consisting of a two fabricated carbon aerogel electrodes (3.0 cm x 2.5 cm x 200 µm) parallel and separated from each other using a commercial AEM and an insulating plate. The 200 ppm NaCl feed water solution was pumped at a constant rate of 20 mL min^{-1} through the CDI cell. The inlet conductivity was measured until constant specific conductivity. After that, a 1.2 V potential was applied to the CDI cell, and the decreasing specific conductivity was measured every 30 seconds until constant values were reached. Salt adsorption capacity (SAC) and salt adsorption rate (SAR) were calculated using Eqs. 5 and 6:

$$SAC = \frac{(C_0 - C_t)\times V}{m} \quad (5)$$

$$SAR = \frac{SAC}{t} \quad (6)$$

with SAC being the salt adsorption capacity (mg g^{-1}); SAR being the salt adsorption rate (mg g^{-1} min^{-1}); C_0, C_t and C_c being the NaCl solution concentration (mg L^{-1}) calculated from the solution specific conductivity at the beginning, at t minutes and at the end, respectively; V being the NaCl solution volume (L); m being the electrode mass (g); and t being the adsorption time (minutes).

3. Results and discussion

3.1 Characterization of SB-ACCA-x materials

Fig. 2 displays the FTIR spectra of the waste- sugarcane-bagasse-derived materials. In Fig. 2a, the intramolecular

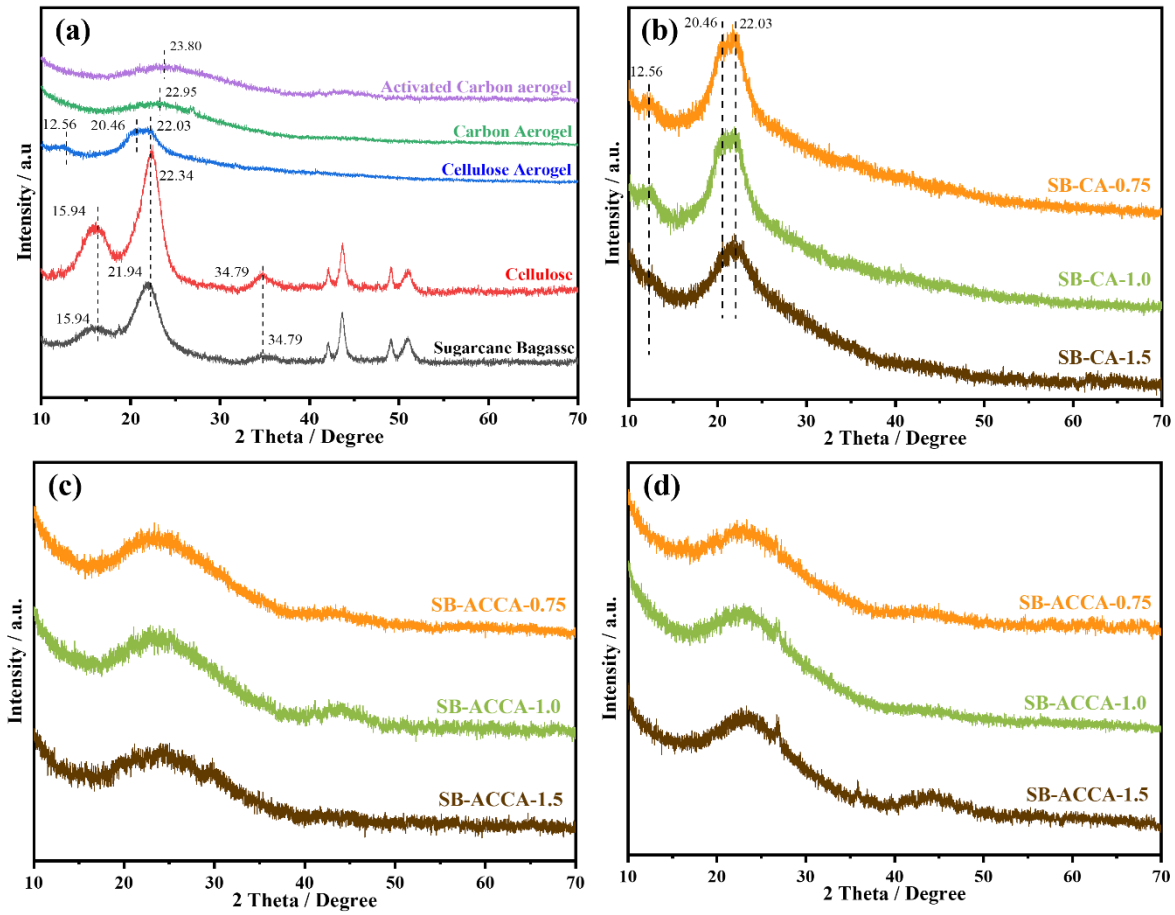

Fig. 3 XRD patterns of (a) different waste-sugarcane-bagasse-derived materials, (b) SB-CA-x, (c) SB-CCA-x, and (d) SB-ACCA-x materials

hydrogen bonding was observed at 3338 cm^{-1}, C–H stretching in the cellulose compounds was detected at 2897 cm^{-1} (Kathirselvam *et al.* 2019, Reddy *et al.* 2014), the bending mode of adsorbed water was observed at 1639 cm^{-1} (Morán *et al.* 2007, Rosa *et al.* 2012, Szcześniak *et al.* 2007), CH_2 bending vibration was found at 1428 cm^{-1} (He *et al.* 2018), OH bending may be at 1376cm^{-1} (Sun *et al.* 2004b), the C-O asymmetric bridge stretching was detected at 1101 and 1160 cm^{-1} (Sun *et al.* 2004b), and the C-O-C pyranose ring vibration was found at 1036 cm^{-1} (Sun *et al.* 2004b). The peak at 831 cm^{-1} in the sugarcane bagasse, which was due to glycosidic linkages between sugar units, was not observed in SB-Cellulose, confirming the removal of sugar thanks to the boiling step in the purification process (Oliveira *et al.* 2017). Similarly, the disappearance of the peak at 1729 cm^{-1} indicated that there were neither the ester linkage of lignin nor the acetyl and uronic ester groups of hemicelluloses in the structure of SB-Cellulose (Sun *et al.* 2005), suggesting that lignin and hemicelluloses were totally eliminated after the basic and acidic treatment. In the FT-IR spectra of cellulose aerogel using different cellulose: urea ratio (Fig. 2b), four main cellulose bands can be detected as mentioned above. After the gelation process, the aforementioned bands underwent the “red shift” to the lower region, which was due to inter- and intra- fibrillar swelling of cellulose caused by the gelation process with the NaOH – urea mixture (Cai and Zhang 2005, Schimper *et al.* 2011). The gelation process also leads to a structural change from cellulose I to cellulose II (Oh *et al.* 2005). Moreover, there may be a new urea functional group (RHN–CO–NHR) peak at 1641 cm^{-1}, which may overlap with the aforementioned 1639 cm^{-1} peak (Baldanza *et al.* 2018). It can be concluded that the gelation process using the NaOH – urea mixture played a vital part in forming the cellulose aerogel structure and changing the characteristics of the cellulose structure.

Fig. 3 displays the XRD patterns of the waste-sugarcane-bagasse-derived materials, showing the characteristic cellulose I peaks at 2θ = 15.94°, 22.34°, and 34.79°, which corresponded to the (110), (200) and (004) planes (Bano and Negi 2017), respectively. Additionally, the intensity of the cellulose peaks in SB-Cellulose increased compared to the sugarcane bagasse, indicating that there was less lignin, since the intensities of the peaks would decrease if the lignin content in cellulose sample increased (Fig. 3a) (Wang *et al.* 2012b). Fig. 3b exhibits the XRD patterns of cellulose aerogel using different cellulose : urea ratio, showing three cellulose II characteristic peaks at 2θ = 12.56, 20.46 and 22.03º, which corresponded to the (1$\bar{1}$0), (110) and (020) lattice planes, respectively (Cai and Zhang 2005, French 2013, Wan and Li 2016, Yu *et al.* 2017). This cellulose I to cellulose II structural change was caused by the dissolution

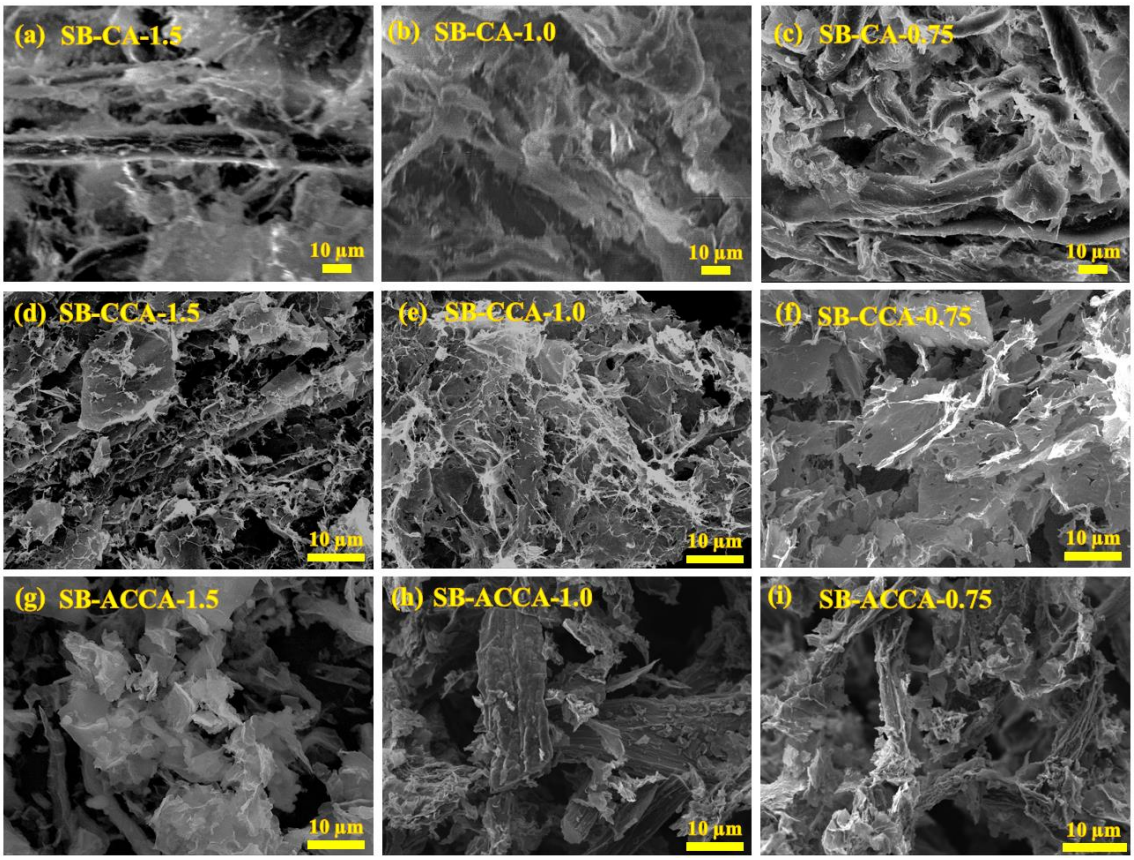

Fig. 4 SEM images of (a,b,c) SB-CA-x, (d, e, f) CCA-x and (g,h,i) SB-ACCA-x materials

Table 2 Surface characterization of SB-ACCA-x materials

Samples	S(BET) (m^2 g^{-1})	S(micropores) (m^2 g^{-1})	S(micropores)/ S(BET) (%)
SB-ACCA-0.75	641.2	556.6	86.80
SB-ACCA-1.0	642.3	434.2	67.60
SB-ACCA-1.5	411.8	321.9	78.17

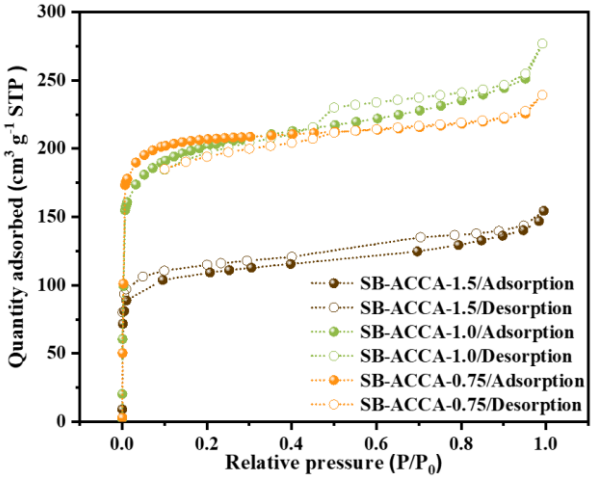

Fig. 5 BET nitrogen adsorption-desorption isotherm plot of SB-ACCA-x materials

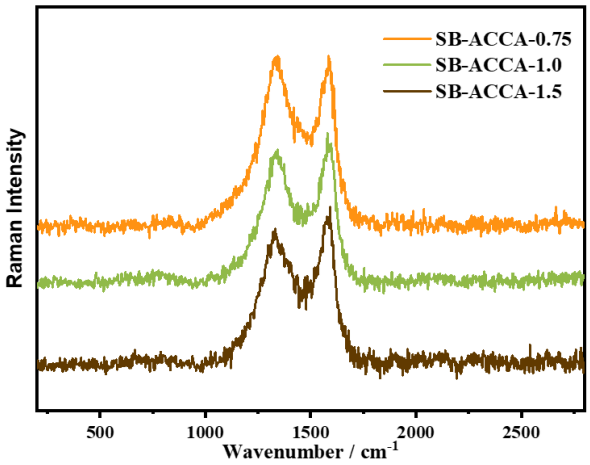

Fig. 6 Raman spectra of SB-ACCA-x materials

of cellulose into the low-temperature solution of NaOH and urea (Chen *et al*. 2015, Wan *et al*. 2019). After carbonization (Fig. 3c), there were two characteristic carbon aerogel peaks at 2θ = 23.5 and 43.7°, which were accredited to the (002) and (100) planes (Seifi *et al*. 2016). Moreover, all of the board diffraction peaks indicated the amorphous carbon structure and disordered graphite microcrystals of the carbon aerogel samples. After KOH activation (Fig. 3d), there was a sharp small peak at 2θ = 26.85º, which is the distinguishable (002) peak of graphite (Siburian *et al*. 2018), indicating an increase in ordered structure of activated carbon aerogel samples.

SEM images of the SB-CA samples (Fig. 4a–c) show the bird's nest structure, which is the hydrogen-bonded network structure between surea and cellulose, as explained

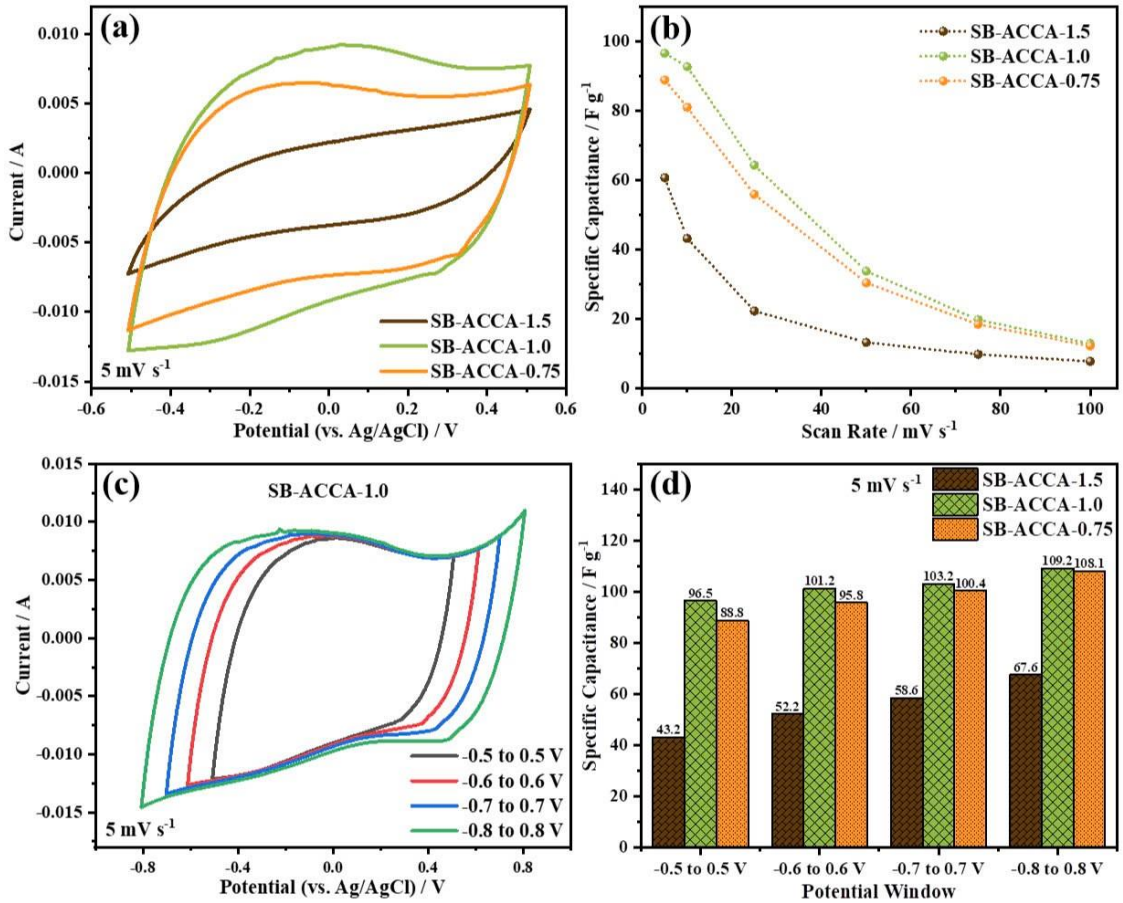

Fig. 7 (a) CV plots of SB-ACCA-x electrodes at 5 mV s^{-1}, (b) specific capacitance values at different scan rate, (c) CV plots of SB-ACCA-1.0 at different potential window and (d) specific capacitance values at different potential window

in our previous research (Nguyen *et al*. 2024). The particle size decreased dramatically and the three-dimensional porous structure collapsed after carbonization and activation (Fig. 4d-i), which was caused by the structural shrinkage due to the aggregation of the internal hydroxyl groups as well as the intermolecular hydrogen bonds at high temperature (Gu *et al*. 2022).

The N_2 adsorption–desorption isotherms of the SB-ACCA samples are presented in Fig. 5, and their corresponding specific surface areas are presented in Table 2. According to the IUPAC classification, all of the SB-ACCA samples exhibited an isotherm of type I with a hysteresis loop of type H4, commonly observed for carbonaceous materials possessing both micropores and mesopores (Kaneko 1994, Linares-Solano *et al*. 2016). Among the samples, SB-ACCA-1.0 exhibited the highest surface area of 642.3 m^2 g^{-1} with 67.60% of micropore surface area (434.2 m^2 g^{-1}), followed by SB-ACCA-0.75 with a surface area of 641.2 m^2 g^{-1} and a micropore percentage of 86.80% (556.6 m^2 g^{-1}). Higher urea content (SB-ACCA-1.5) resulted in a lower specific surface area but a higher percentage of micropores compared to SB-ACCA-1.0. Urea, when incorporated into the cellulose structure, can act as a plasticizer by disrupting the hydrogen bonds between cellulose chains. This disruption enhances the flexibility of the cellulose matrix, facilitating the formation of smaller cellulose chains as well as more number of micropores during the gelation process (Abas and Attia 2023). Moreover, urea can also act as a cross-linking agent by forming hydrogen bonds with cellulose chains (Nguyen *et al*. 2024). This cross-linking effect restricts the mobility of the cellulose chains, leading to a denser and more compact structure during the carbonization and activation processes. As a result, the formation of larger mesopores is hindered, while the development of smaller, more uniform micropores is promoted. Additionally, during the activation process, the presence of urea can influence the decomposition pathway of cellulose. The cross-linked structure may favor the generation of micropores by creating localized regions of higher thermal stability, which resist collapse into larger pores. This mechanism explains the observed increase in micropore percentage and the corresponding decrease in mesopore and macropore volume, which contribute significantly to the lower specific surface area. The BET results corresponded well with the aforementioned SEM images.

Comparison of Raman spectra of the SB-ACCA-x is shown in Fig. 6, showing two noticeable peaks were at 1331 and 1581 cm^{-1}. The D-band at 1331 cm^{-1} corresponds to defective graphitic structures, while the G-band at 1581 cm^{-1} corresponds to the graphitic composition of samples (Ferrari and Robertson 2000). The relative intensities of these two bands (I_D/I_G) indicates the degree of disorder and defects in carbons (Jawhari *et al*. 1995). Specifically, I_D/I_G

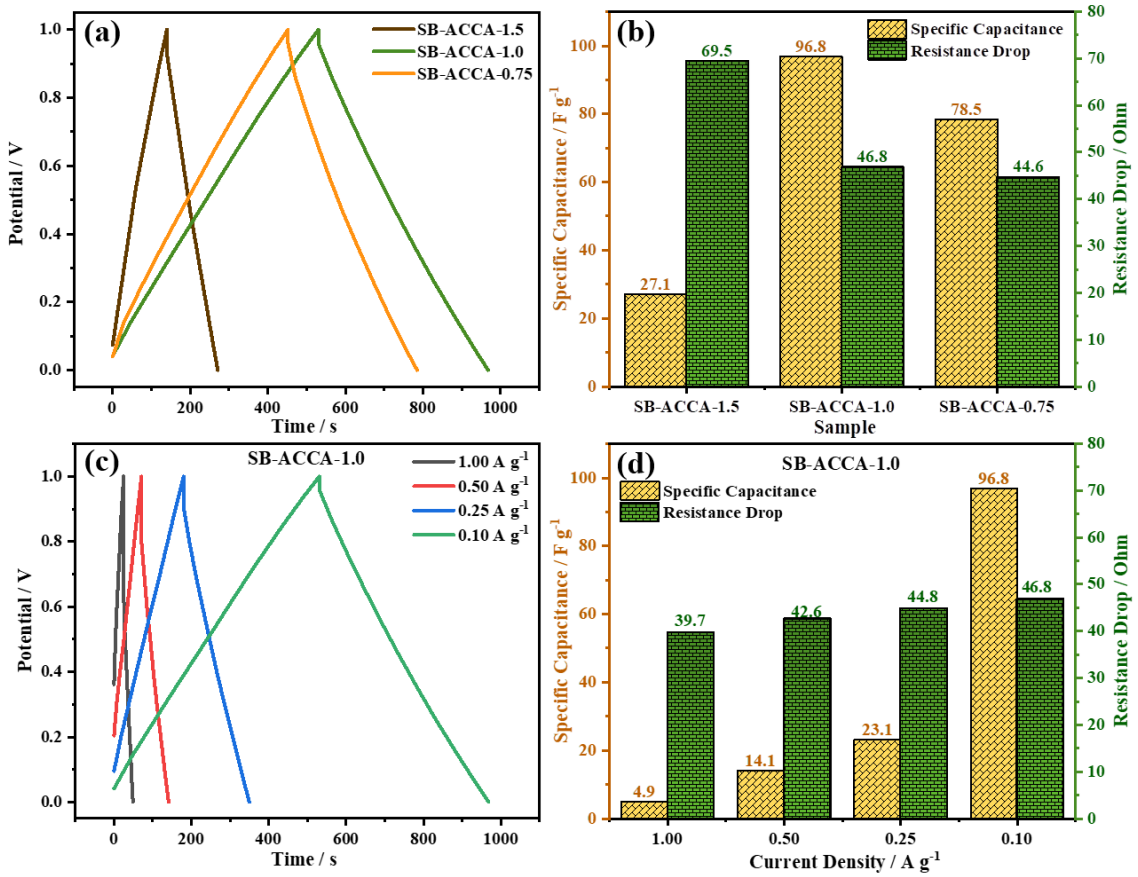

Fig. 8 (a) GCD plots and (b) specific capacitance and resistance drop values at different scan rate of SB-ACCA-x electrodes, (c) GCD plots and (d) specific capacitance and resistance drop values at different current densities of SB-ACCA-1.0

values of SB-ACCA-0.75, SB-ACCA-1.0 and SB-ACCA-1.5 are 1.05, 0.91 and 0.93, respectively (Table 3). The increase in the urea content led to a decrease in the I_D/I_G value, indicating a somewhat higher degree of structural order in the carbon aerogel samples. This result agrees well with XRD results.

3.2 Characterization of SB-ACCA-x electrodes

The CV diagrams of the SB-ACCA electrodes are presented in Fig. 7a, showing a nearly rectangular shape, which indicated that the double layer effect dominated the capacitive behavior of the electrode. It can be observed that, with the scan rate increasing from 5 to 100 mV s^{-1}, the specific capacitance values of SB-ACCA-0.75, SB-ACCA-1.0 and SB-ACCA-1.5 electrodes gradually decreased from 88.8, 96.5 and 49.5 F g^{-1} to 12.21, 12.87 and 7.79 F g^{-1}, respectively (Fig. 7b). This is because the lower scan rate will provide the ions with more time to diffuse from the solution to the pores of the electrode (Quan *et al*. 2017). The CV curves SB-ACCA-1.0 electrode at 5 mV s^{-1} at various potential windows (from -0.5 – 0.5 V to -0.8 – 0.8 V) are shown in Fig. 7c. It can be seen that the quasi-rectangular shape of the CV curves remain unchanged, suggesting that the SB-ACCA-1.0 electrode can exhibit good supercapacitive behavior and work well even at high potential window like 1.6 V (Mohd Abdah *et al*. 2019). The specific capacitance value of SB-ACCA-1.0 is superior at all potential windows (Fig. 7d). Additionally, the specific capacitance values of SB-ACCA-x electrodes increased when the potential window was widened, although there was not much difference. However, as the potential window increased, there were some changes at both of the oxidation and reduction ends. This phenomenon was due to the water reduction at -0.85 V and water oxidation at 0.8 V (Hendel and Young 2016), which are undesirable reactions. Therefore, it is best to conduct the electrosorption processes at a smaller potential window of less than 1.6 V.

From the GCD curves of SB-ACCA-x electrodes (Fig. 8a) and those of SB-ACCA-1.0 electrode recorded at different current densities (Fig. 8c), the GCD curves are observed to show typical nearly symmetrical triangular shape, indicating perfect double layer capacitor properties. These results agrees well with the CV results as discussed above. Moreover, the specific capacitance values calculated from the GCD curves were nearly similar to those determined from the CV curves (Fig 8b). SB-ACCA-1.5 electrode exhibit a higher resistance drop (69.5 Ω) compared to SB-ACCA-0.75 and SB-ACCA-1.0 (46.8 and 44.6 Ω, respectively), which may be resulted from the crosslinked structure (Huo *et al*. 2019). The increase in the urea amount as the cross-linking agent may lead to the decrease in the number of mesopores (which decrease electron mobility) as well as the increase the number of

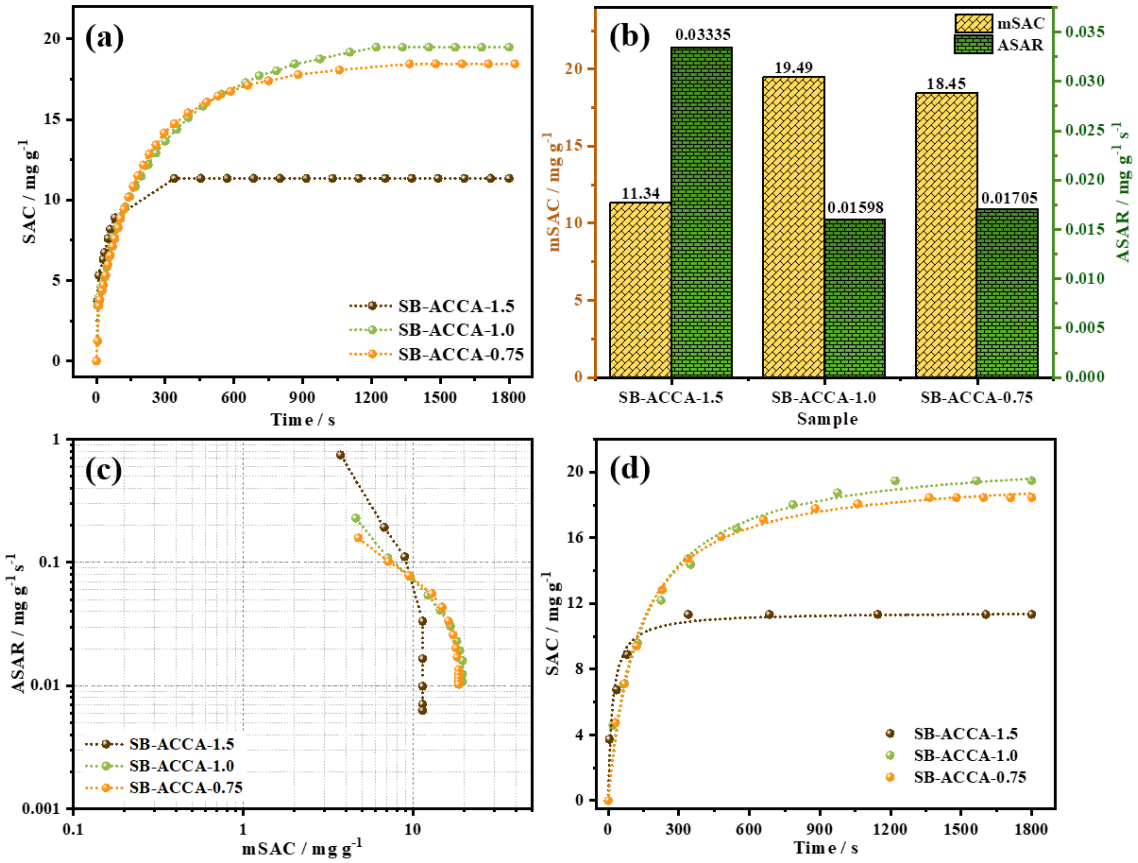

Fig. 9 (a) The SAC value as a function of desalination time, (b) mSAC and ASAR values, (c) Kim-Yoon plots and (d) kinetics of the adsorption process for MCDI process using SB-ACCA-x electrodes

Table 4 parameters of first- and second-order kinetic models for mcdi process using sb-acca-x electrodes

SAMPLE	First order			Second order		
	mSAC (mg g^{-1})	K (s^{-1})	R^2	mSAC (mg g^{-1})	K (mg g^{-1} s^{-1})	R^2
SB-ACCA-1.5	11.21	0.0267	0.9531	11.48	4.73 x 10^{-3}	0.9808
SB-ACCA-1.0	18.81	0.00517	0.9668	21.17	3.302 x 10^{-4}	0.9883
SB-ACCA-0.75	18.06	0.0059	0.9848	19.98	4.105 x 10^{-4}	0.9974

micropores (which allow more electrons to be trapped in the tortuous paths) (Armatas 2006, Díaz-Curiel *et al.* 2021), thus increase the resistance values. Additionally, the current densities greatly affected the specific capacitance values of the electrode, as the specific capacitance decreased from 96.8 to 4.9 F g^{-1} with the current density increasing from 0.1 to 1.0 A g^{-1} (Fig. 8d). This phenomenon could be caused by the reduced ability of the electrode to use their active surface at elevated current densities (Raavi *et al.* 2023).

3.3 Capacitive deionization desalination using waste-sugarcane-bagasse-derived carbon aerogel electrode

As observed in Fig. 9a, the maximum SAC (mSAC) values for the SB-ACCA-0.75, SB-ACCA-1.0 and SB-ACCA-1.5 electrodes were 18.45, 19.49 and 11.34 mg g^{-1}, respectively, which was consistent with the properties investigated previously such as the specific surface area, specific capacitance and resistance drop. However, the average salt adsorption rate inferred from the adsorption curve of the SB-ACCA-1.0 sample was lower than that of the SB-ACCA-1.5 electrode (Fig. 9b). The reason was that, at the initial stage, the adsorption rates of the electrodes were similar, but due to poor adsorption capacity of the SB-ACCA-1.5 electrode, the desalination process quickly saturated at about 340 seconds to reach 11.34 mg g^{-1}, while the process using SB-ACCA-1.0 electrode saturated at 1220 seconds with a significantly higher mSAC value. This can be observed more clearly through the Kim-Yoon diagram (Fig. 9c), as the SB-ACCA-1.0 and SB-ACCA-0.75 electrodes have superior mSAC and ASAR values compared to the SB-ACCA-1.5 electrode.

The kinetics of NaCl adsorption process was investigated. As observed in Fig. 9d and Table 4, the coefficients of determination of the second-order kinetic model are higher compared to that of the first-order kinetic model (R^2 = 0.9808 – 0.9974 compared to 0.9531 – 0.9848), and the

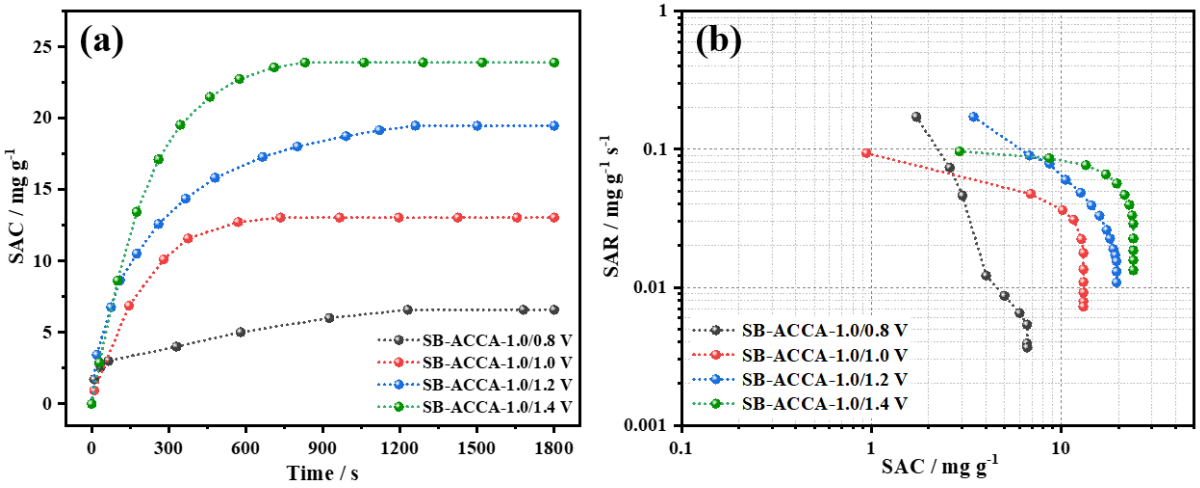

Fig. 10 (a) The SAC value as a function of desalination time and (b) Kim-Yoon plots for MCDI process using SB-ACCA-1.0 electrode at different potentials

mSAC value derived from the second-order kinetic model corresponds to the actual value. Therefore, it can be concluded that the adsorption process of salt ions onto the waste-sugarcane-bagasse-derived carbon aerogel electrodes through the capacitive deionization system is more consistent with the second-order kinetic model rather than with the first-order kinetic model.

The desalination process was then conducted using SB-ACCA-1.0 electrode at different charged potential (Fig. 10). Higher potential resulted in higher mSAC value, as it increased from 6.59 mg g^{-1} at 0.8 V to 23.91 mg g^{-1} at 1.4 V, together with a higher ASAR values. This result can be explained that higher potential could generate stronger electrostatic interaction, thus it is able to adsorb greater amount of salt ions.

4. Conclusions

In this study, cellulose aerogel was fabricated from waste sugarcane bagasse using the NaOH/Urea/H_2O gelation solution with different amount of urea, then was carbonized and activated to acquire activated cellulose carbon aerogel. The best materials with the cellulose : urea ratio of 1 : 1, denoted as SB-ACCA-1.0, exhibited the highest specific surface area of 642.3 m^2 g^{-1} with 67.60% of micropore surface area (434.2 m^2 g^{-1}) and the highest specific capacitance value of 96.5 F g^{-1}, resulting in a high salt adsorption capacity of 19.49 mg g^{-1} at 1.2 V, which can be enhanced to 23.91 mg g^{-1} at 1.4 V. This result suggests a potential application of cellulose carbon aerogel derived from waste sugarcane bagasse as well as other biomass and biowaste as a potential material for MCDI-utilized electrode for the desalination of salt water.

Acknowledgments

This research was funded by NTTU Foundation for Science and Technology Development under grant number 2024.01.111/HĐ-KHCN.

References

Abas, K.M. and Attia, A.A.M. (2023), "Thermoplastic starch (TPS)-based composite films for wastewater treatment: synthesis and fundamental characterization", *BMC Chem*., **17**(1), 84. https://doi.org/10.1186/s13065-023-00998-z

Ahamad, T., Naushad, M., Ruksana, Alhabarah, A.N. and Alshehri, S.M. (2019), "N/S doped highly porous magnetic carbon aerogel derived from sugarcane bagasse cellulose for the removal of bisphenol-A", *Int. J. Biol. Macromol*., **132**, 1031-1038. https://doi.org/10.1016/j.ijbiomac.2019.04.004

Ajala, E.O., Ighalo, J.O., Ajala, M.A., Adeniyi, A.G. and Ayanshola, A.M. (2021), "Sugarcane bagasse: a biomass sufficiently applied for improving global energy, environment and economic sustainability", *Bioresour. Bioproc*., **8**(1), 87. https://doi.org/10.1186/s40643-021-00440-z

Alokika, Anu, Kumar, A., Kumar, V. and Singh, B. (2021), "Cellulosic and hemicellulosic fractions of sugarcane bagasse: Potential, challenges and future perspective", *Int. J. Biol. Macromol*., **169**, 564-582. https://doi.org/10.1016/j.ijbiomac.2020.12.175

Anovitz, L.M. and Cole, D.R. (2015), "Characterization and analysis of porosity and pore structures", *Rev. Mineral. Geochem*., **80**(1), 61-164. https://doi.org/10.2138/rmg.2015.80.04

Anukam, A., Mamphweli, S., Reddy, P., Meyer, E. and Okoh, O. (2016), "Pre-processing of sugarcane bagasse for gasification in a downdraft biomass gasifier system: A comprehensive review", *Renew. Sust. Energy Rev*., **66**, 775-801. https://doi.org/10.1016/j.rser.2016.08.046

Armatas, G.S. (2006), "Determination of the effects of the pore size distribution and pore connectivity distribution on the pore tortuosity and diffusive transport in model porous networks", *Chem. Eng. Sci*., **61**(14), 4662-4675. https://doi.org/10.1016/j.ces.2006.02.036

Arni, S.A. (2018), "Extraction and isolation methods for lignin separation from sugarcane bagasse: A review", *Ind. Crops Prod*., **115**, 330-339. https://doi.org/10.1016/j.indcrop.2018.02.012

Baldanza, V.A.R., Souza, F.G., Filho, S.T., Franco, H.A., Oliveira, G.E., Caetano, R.M.J., Hernandez, J.A.R., Ferreira Leite, S.G., Furtado Sousa, A.M. and Nazareth Silva, A.L. (2018), "Controlled-release fertilizer based on poly(butylene succinate)/urea/clay and its effect on lettuce growth", *J. Appl. Polym. Sci*., **135**(47). https://doi.org/10.1002/app.46858

Bano, S. and Negi, Y.S. (2017), "Studies on cellulose nanocrystals isolated from groundnut shells", *Carbohydr. Polym.*, **157**, 1041-1049. https://doi.org/10.1016/j.carbpol.2016.10.069

Bhatnagar, A., Kesari, K.K. and Shurpali, N. (2015), "Multidisciplinary Approaches to Handling Wastes in Sugar Industries", *Water Air Soil Pollut.*, **227**(1). https://doi.org/10.1007/s11270-015-2705-y

Cai, J. and Zhang, L. (2005), "Rapid dissolution of cellulose in LiOH/urea and NaOH/urea aqueous solutions", *Macromol Biosci.*, **5**(6), 539-48. https://doi.org/10.1002/mabi.200400222

Chen, X., Chen, J., You, T., Wang, K. and Xu, F. (2015), "Effects of polymorphs on dissolution of cellulose in NaOH/urea aqueous solution", *Carbohydr. Polym.*, **125**, 85-91. https://doi.org/10.1016/j.carbpol.2015.02.054

Díaz-Curiel, J., Biosca, B., Arévalo-Lomas, L. and Miguel, M.J. (2021), "Failure of the conventional expression of tortuosity in granular porous solids", *Surveys Geophys.*, **42**(4), 943-960. http://doi.org/10.1007/s10712-021-09645-5

El-Gendi, A., Ali, S.S., Ahmed, S.A. and Talaat, H.A. (2012), "Development of membrane blend using casting technique for water desalination", *Membr. Water Treat.*, **3**(3), 201-209. https://doi.org/10.12989/mwt.2012.3.3.201

Ferrari, A.C. and Robertson, J. (2000), "Interpretation of Raman spectra of disordered and amorphous carbon", *Phys. Rev. B*, **61**(20), 14095-14107. https://doi.org/10.1103/PhysRevB.61.14095

French, A.D. (2013), "Idealized powder diffraction patterns for cellulose polymorphs", *Cellulose*, **21**(2), 885-896. https://doi.org/10.1007/s10570-013-0030-4

Gu, H., Huo, X., Chen, J., El-Bahy, S.M. and El-Bahy, Z.M. (2022), "An overview of cellulose aerogel: classification and applications", *ES Food Agroforest.*, **10**, 1-9. http://doi.org/10.30919/esfaf782

He, Q., Wang, Q., Zhou, H., Ren, D., He, Y., Cong, H. and Wu, L. (2018), "Highly crystalline cellulose from brown seaweed Saccharina japonica: isolation, characterization and micro-crystallization", *Cellulose*, **25**(10), 5523-5533.

Hendel, S.J. and Young, E.R. (2016), "Introduction to electrochemistry and the use of electrochemistry to synthesize and evaluate catalysts for water oxidation and reduction", *J. Chem. Educ.*, **93**(11), 1951-1956. https://doi.org/10.1021/acs.jchemed.6b00230

Hiranobe, C.T., Gomes, A.S., Paiva, F.F.G., Tolosa, G.R., Paim, L.L., Dognani, G., Cardim, G.P., Cardim, H.P., dos Santos, R.J. and Cabrera, F.C. (2024), "Sugarcane bagasse: Challenges and opportunities for waste recycling", *Clean Technologies*, **6**(2), 662-699. https://doi.org/10.3390/cleantechnol6020035

Huo, P., Ni, S., Hou, P., Xun, Z., Liu, Y. and Gu, J. (2019), "A crosslinked soybean protein isolate gel polymer electrolyte based on neutral aqueous electrolyte for a high-energy-density supercapacitor", *Polymers*, **11**(5). https://doi.org/10.3390/polym11050863

Jawhari, T., Roid, A. and Casado, J. (1995), "Raman spectroscopic characterization of some commercially available carbon black materials", *Carbon*, **33**(11), 1561-1565. https://doi.org/10.1016/0008-6223(95)00117-V

Kaneko, K. (1994), "Determination of pore size and pore size distribution", *J. Membr. Sci.*, **96**(1-2), 59-89. https://doi.org/10.1016/0376-7388(94)00126-X

Karp, S.G., Woiciechowski, A.L., Soccol, V.T. and Soccol, C.R. (2013), "Pretreatment strategies for delignification of sugarcane bagasse: a review", *Brazil. Arch. Biol. Technol.*, **56**(4), 679-689. https://doi.org/10.1590/S1516-89132013000400019

Katariya, H.N. and Pate, T.M. (2022), "Cellulose acetate membrane preparation by phase inversion to estimate optimized parameters and its performance study", *Membr. Water Treat.*, **13**(3), 139-145. https://doi.org/10.12989/mwt.2022.13.3.139

Kathirselvam, M., Kumaravel, A., Arthanarieswaran, V.P. and Saravanakumar, S.S. (2019), "Isolation and characterization of cellulose fibers from *Thespesia populnea* barks: A study on physicochemical and structural properties", *Int. J. Biol. Macromol.*, **129**, 396-406. https://doi.org/10.1016/j.ijbiomac.2019.02.044

Kim, J.S. and Rhim, J.W. (2016), "Comparison of CDI and MCDI applied with sulfonated and aminated polysulfone polymers", *Membr. Water Treat.*, **7**(1), 39-53. https://doi.org/10.12989/mwt.2016.7.1.039

Kumar, G., Dora, D.T.K., Jadav, D., Naudiyal, A., Singh, A. and Roy, T. (2021), "Utilization and regeneration of waste sugarcane bagasse as a novel robust aerogel as an effective thermal, acoustic insulator, and oil adsorbent", *J. Clean. Prod.*, **298**, 126744. https://doi.org/10.1016/j.jclepro.2021.126744

Lei, Y., Sun, W., Tiwari, S.K., Thummavichai, K., Ola, O., Qin, X., Ma, Z., Wang, N. and Zhu, Y. (2021), "Zn/Co-ZIF reinforced sugarcane bagasse aerogel for highly efficient catalytic activation of peroxymonosulfate", *J. Environ. Chem. Eng.*, **9**(6), https://doi.org/10.1016/j.jece.2021.106885

Lemessa, G., Gabbiye, N. and Alemayehu, E. (2023), "Waste to resource: Utilization of waste bagasse as an alternative adsorbent to remove heavy metals from wastewaters in sub-Saharan Africa: A review", *Water Pract. Technol.*, **18**(2), 393-407. https://doi.org/10.2166/wpt.2023.011

Li, W., Li, Z., Wang, W., Li, Z., Li, Q., Qin, C. and Cao, F. (2021a), "Green approach to facilely design hydrophobic aerogel directly from bagasse", *Ind. Crops Prod.*, **172**, 113957. https://doi.org/10.1016/j.indcrop.2021.113957

Li, Z., Lei, S., Xi, J., Ye, D., Hu, W., Song, L., Hu, Y., Cai, W. and Gui, Z. (2021b), "Bio-based multifunctional carbon aerogels from sugarcane residue for organic solvents adsorption and solar-thermal-driven oil removal", *Chem. Eng. J.*, **426**, 129580. https://doi.org/10.1016/j.cej.2021.129580

Linares-Solano, A., Rodríguez-Reinoso, F., Martín-Martínez, J.M. and López-González, J.D. (2016), "Adsorption of Hydrocarbons on Air-Reacted Activated Carbons. II. High and Low Pressure Hysteresis", *Adsorpt. Sci. Technol.*, **1**(4), 317-327. http://doi.org/10.1177/026361748400100405

Mohd Abdah, M.A.A., Azman, N.H.N., Kulandaivalu, S. and Sulaiman, Y. (2019), "Asymmetric supercapacitor of functionalised electrospun carbon fibers/poly(3,4-ethylenedioxythiophene)/ manganese oxide//activated carbon with superior electro-chemical performance", *Sci Rep*, **9**(1), 16782. https://doi.org/10.1038/s41598-019-53421-w

Morán, J.I., Alvarez, V.A., Cyras, V.P. and Vázquez, A. (2007), "Extraction of cellulose and preparation of nanocellulose from sisal fibers", *Cellulose*, **15**(1), 149-159. http://doi.org/10.1007/s10570-007-9145-9

Ngo, H.L., Nguyen, N.T., Ho, T.T.N., Pham, H.V., Tran, T.N., Huynh, L.T.N., Pham, T.N., Nguyen, T.T., Nguyen, T.H., Le, V.H. and Tran, D.L. (2022), "A low-cost and eco-friendly fabrication of an MCDI-utilized PVA/SSA/GA cation exchange membrane", *Green Process. Synth.*, **11**(1), 563-571. https://doi.org/10.1515/gps-2022-0056

Nguyen, N.T., Duong, T.T.T., Phan, T.V.T., Truong, C.C., Nguyen, V.V., Tran, T.N., Nguyen, T.T., Anh, T.H., Hoang, S.M.T., Ngo, H.L. and Chung, N.T.K. (2023a), "Water hyacinth as a green and sustainable material for carbon aerogel electrodes utilized in membrane capacitive deionization", *Clean Soil Air Water*, **51**(8), 2200396.https://doi.org/10.1002/clen.202200396

Nguyen, T.H., Nguyen, V.V., Nguyen, N.T., Nguyen, T., Nguyen, T.V.T., Ngo, H.L., Huynh, L.T.N., Tran, T.N., Ho, T.T.N., Nguyen, T.T. and Le, V.H. (2022a), "Preparation, characterization and CDI application of KOH-activated porous waste-corn-stalk-based carbon aerogel", *J. Porous Mater.*, **30**, 1183-1193. https://doi.org/10.1007/s10934-022-01411-1

Nguyen, T.T., Hoang, Q.T., Nguyen, T.T., Pham, T.A., Cao, A.D., Pham, H.D., Le, V.H., Vu, T.T., Pham, N.H., Nguyen, T.C., To, K.A., Nguyen, V.H., Phi, Q.T., Tran, V.H., Dang, T.T., Lai, Q.D., Lionnet, R. and Chu-Ky, S. (2022b), "Research and development prospects for sugarcane industry in Vietnam", *Sugar Tech*., 1-12. https://doi.org/10.1007/s12355-022-01113-7

Nguyen, T.T., Nguyen, N.T., Nguyen, V.V., Nguyen, A.H., Hoang Tran, B.D., Vo, T.K., Truong, D.T., Doan, T.L.H., Huynh, L.T.N., Tran, T.N., Ngo, H.L., Le, V.H. and Nguyen, T.H. (2024), "Tailoring hierarchical structures in cellulose carbon aerogels from sugarcane bagasse using different crosslinking agents for enhancing electrochemical desalination capability", *Chemosphere*, **355**, 141748. https://doi.org/10.1016/j.chemosphere.2024.141748

Nguyen, T.V.T., Nguyen, N.T., Nguyen, V.V., Nguyen, T., Ngo, H.L., Huynh, L.T.N., Le, H.C., Tran, T.N., Ho, T.T.N., Nguyen, T.T., Le, V.H. and Nguyen, T.H. (2023b), "Effect of urea content on MCDI performance of waste-corn-stalk-derived cellulose carbon aerogel", *Fibers Polym*., **24**(6), 1929-1939. https://doi.org/10.1007/s12221-023-00234-4

Oh, S.Y., Yoo, D.I., Shin, Y. and Seo, G. (2005), "FTIR analysis of cellulose treated with sodium hydroxide and carbon dioxide", *Carbohydr*. *Res*., **340**(3), 417-428. https://doi.org/10.1016/j.carres.2004.11.027

Oliveira, J.P., Bruni, G.P., Lima, K.O., Halal, S., Rosa, G.S.D., Dias, A.R.G. and Zavareze, E.D.R. (2017), "Cellulose fibers extracted from rice and oat husks and their application in hydrogel", *Food Chem*, **221**, 153-160. https://doi.org/10.1016/j.foodchem.2016.10.048

Ong, S.T., Khoo, E.C., Hii, S.L. and Ha, S.T. (2010), "Utilization of sugarcane bagasse for removal of basic dyes from aqueous environment in single and binary systems", *Desalin. Water Treat*., **20**(1-3), 86-95. https://doi.org/10.1080/19443994.2010.10513772

Quan, X., Fu, Z., Yuan, L., Zhong, M., Mi, R., Yang, X., Yi, Y. and Wang, C. (2017), "Capacitive deionization of NaCl solutions with ambient pressure dried carbon aerogel microsphere electrodes", *RSC Adv*., **7**(57), 35875-35882. https://doi.org/10.1039/C7RA05226J

Raavi, R., Archana, S., Adinarayana Reddy, P. and Elumalai, P. (2023), "Performances of dual carbon multi-ion supercapacitors in aqueous and non-aqueous electrolytes", *Energy Adv*., **2**(3), 385-397. https://doi.org/10.1039/D2YA00271J

Reddy, K.O., Ashok, B., Reddy, K.R.N., Feng, Y.E., Zhang, J. and Rajulu, A.V. (2014), "Extraction and characterization of novel lignocellulosic fibers from thespesia lampas plant", *Int*. *J*. *Polym*. *Anal*. *Character*., **19**(1), 48-61. https://doi.org/10.1080/1023666X.2014.854520

Rosa, S.M.L., Rehman, N., de Miranda, M.I.G., Nachtigall, S.M.B. and Bica, C.I.D. (2012), "Chlorine-free extraction of cellulose from rice husk and whisker isolation", *Carbohydr*. *Polym*., **87**(2), 1131-1138. https://doi.org/10.1016/j.carbpol.2011.08.084

Safa, Y., Tariq, S.R., Bhatti, H.N., Sultan, M., Bibi, I. and Nouren, S. (2018), "Synthesis and characterization of sugarcane bagasse/zinc aluminium and apple peel/zinc aluminium biocomposites: Application for removal of reactive and acid dyes", *Membr*. *Water Treat*., **9**(5), 301-307. https://doi.org/10.12989/mwt.2018.9.5.301

Schimper, C.B., Ibanescu, C. and Bechtold, T. (2011), "Surface activation of dyed fabric for cellulase treatment", *Biotechnol J*, **6**(10), 1280-1285. http://doi.org/10.1002/biot.201100002

Seifi, A., Bahramian, A.R. and Sharif, A. (2016), "Correlation between structure and oxidation behavior of carbon aerogels", *J*. *Energy Storage*, **7**, 195-203. https://doi.org/10.1016/j.est.2016.07.003

Shi, G., Qian, Y., Tan, F., Cai, W., Li, Y. and Cao, Y. (2019), "Controllable synthesis of pomelo peel-based aerogel and its application in adsorption of oil/organic pollutants", *R Soc Open Sci*, **6**(2), 181823. https://doi.org/10.1098/rsos.181823

Siburian, R., Sihotang, H., Lumban Raja, S., Supeno, M. and Simanjuntak, C. (2018), "New route to synthesize of graphene nano sheets", *Orient*. *J*. *Chem*., **34**(1), 182-187. http://doi.org/10.13005/ojc/340120

Sun, J.X., Sun, X.F., Zhao, H. and Sun, R.C. (2004a), "Isolation and characterization of cellulose from sugarcane bagasse", *Polym. Degrad*. *Stabil*., **84**(2), 331-339. https://doi.org/10.1016/j.polymdegradstab.2004.02.008

Sun, W., Thummavichai, K., Chen, D., Lei, Y., Pan, H., Song, T., Wang, N. and Zhu, Y. (2021), "Co-zeolitic imidazolate framework@cellulose aerogels from sugarcane bagasse for activating peroxymonosulfate to degrade P-nitrophenol", *Polymers*, **13**(5), https://doi.org/10.3390/polym13050739

Sun, X.F., Sun, R.C., Su, Y. and Sun, J.X. (2004b), "Comparative study of crude and purified cellulose from wheat straw", *J*. *Agric*. *Food Chem*., **52**(4), 839-847. https://doi.org/10.1021/jf0349230

Sun, X.F., Xu, F., Sun, R.C., Fowler, P. and Baird, M.S. (2005), "Characteristics of degraded cellulose obtained from steam-exploded wheat straw", *Carbohydr*. *Res*., **340**(1), 97-106. https://doi.org/10.1016/j.carres.2004.10.022

Szcześniak, L., Rachocki, A. and Tritt-Goc, J. (2007), "Glass transition temperature and thermal decomposition of cellulose powder", *Cellulose*, **15**(3), 445-451. http://doi.org/10.1007/s10570-007-9192-2

Thai, Q.B., Nguyen, S.T., Ho, D.K., Tran, T.D., Huynh, D.M., Do, N.H.N., Luu, T.P., Le, P.K., Le, D.K., Phan-Thien, N. and Duong, H.M. (2020), "Cellulose-based aerogels from sugarcane bagasse for oil spill-cleaning and heat insulation applications", *Carbohydr*. *Polym*., **228**, 115365. https://doi.org/10.1016/j.carbpol.2019.115365

Thiangtham, S., Runt, J. and Manuspiya, H. (2019), "Sulfonation of dialdehyde cellulose extracted from sugarcane bagasse for synergistically enhanced water solubility", *Carbohydr*. *Polym*., **208**, 314-322. https://doi.org/10.1016/j.carbpol.2018.12.080

Tran, V.C., Pham, N.Q., Le, A.K., Tran, A.K. and Pham, C.M. (2022), "Carbon aerogel from jackfruit waste as new material for electrodes capacitive deionization", *Chem*. *Eng*. *Trans*., **97**, 181-186. https://doi.org/10.3303/CET2297031

Wan, C., Jiao, Y., Wei, S., Zhang, L., Wu, Y. and Li, J. (2019), "Functional nanocomposites from sustainable regenerated cellulose aerogels: A review", *Chem*. *Eng*. *J*., **359**, 459-475. https://doi.org/10.1016/j.cej.2018.11.115

Wan, C. and Li, J. (2016), "Incorporation of graphene nanosheets into cellulose aerogels: enhanced mechanical, thermal, and oil adsorption properties", *Appl*. *Phys*. *A*, **122**(2). https://doi.org/10.1007/s00339-016-9641-6

Wang, J., Zheng, Y. and Wang, A. (2012a), "Superhydrophobic kapok fiber oil-absorbent: Preparation and high oil absorbency", *Chem*. *Eng*. *J*., **213**, 1-7. https://doi.org/10.1016/j.cej.2012.09.116

Wang, X., Cui, X. and Zhang, L. (2012b), "Preparation and characterization of lignin-containing nanofibrillar cellulose", *Procedia Environ*. *Sci*., **16**, 125-130. https://doi.org/10.1016/j.proenv.2012.10.017

Wulandari, W.T., Rochliadi, A. and Arcana, I.M. (2016), "Nanocellulose prepared by acid hydrolysis of isolated cellulose from sugarcane bagasse", *IOP Conf*. *Ser*. *Mater*. *Sci*. *Eng*., **107**. https://doi.org/10.1088/1757-899X/107/1/012045

Wuri, M.A., Pertiwiningrum, A., Budiarto, R., Gozan, M. and Harto, A.W. (2021), "The waste recycling of sugarcane bagasse-based biochar for biogas purification", *IOP Conference Series: Earth and Environmental Science*, **940**(1), 012029. https://doi.org/10.1088/1755-1315/940/1/012029

Yang, X., Liu, L. and Jiang, S. (2019), "Enhancement of hydrophilicity and anti-fouling property of polysulfone membrane using amphiphilic nanocellulose as hydrophilic modifier", *Membr. Water Treat.*, **10**(6), 461-469. https://doi.org/10.12989/mwt.2019.10.6.461

Yao, S., Nie, S., Yuan, Y., Wang, S. and Qin, C. (2015), "Efficient extraction of bagasse hemicelluloses and characterization of solid remainder", *Bioresour Technol*, **185**, 21-27. https://doi.org/10.1016/j.biortech.2015.02.052

Yu, M., Li, J. and Wang, L. (2017), "KOH-activated carbon aerogels derived from sodium carboxymethyl cellulose for high-performance supercapacitors and dye adsorption", *Chem. Eng. J.*, **310**, 300-306. https://doi.org/10.1016/j.cej.2016.10.121

KC